Werk

Jahr: 1985
Kollektion: fid.geo
Signatur: 8 Z NAT 2148:57
Digitalisiert: Niedersächsische Staats- und Universitätsbibliothek Göttingen
Werk Id: PPN1015067948_0057
PURL: http://resolver.sub.uni-goettingen.de/purl?PPN1015067948_0057

LOG Id: LOG_0021
LOG Titel: The influence of dirt bands and faults on the propagation of love seam waves
LOG Typ: article

Übergeordnetes Werk

Werk Id: PPN1015067948
PURL: http://resolver.sub.uni-goettingen.de/purl?PPN1015067948
OPAC: http://opac.sub.uni-goettingen.de/DB=1/PPN?PPN=1015067948

Contact

Niedersächsische Staats- und Universitätsbibliothek Göttingen
Georg-August-Universität Göttingen
Platz der Göttinger Sieben 1
37073 Göttingen
Germany
Email: gdz@sub.uni-goettingen.de

J Geophys (1985) 57:77–89

Journal of Geophysics

The influence of dirt bands and faults on the propagation of Love seam waves

C. Kerner and L. Dresen
Institut für Geophysik, Ruhr-Universität Bochum, PO Box 102148, D-4630 Bochum 1, Federal Republic of Germany

Abstract. Discontinuities in a coal seam can be detected by in-seam seismic surveys. However, a detailed understanding of wave propagation in coal seams interlayered with dirt bands can provide a more efficient use of this technique. In addition, improvements in this method are possible if one knows the effect of the fault parameters on the field data.

This paper presents the results from a numerical simulation of the propagation of Love seam waves in two-dimensional heterogeneous geological structures. The frequency content of the source signal and the profiles in the centre of the coal layers correspond to current field techniques. Finite difference methods are used.

The effect of modes higher than the first mode on the propagation of waves in seams which are interlayered with dirt bands was studied. The Airy phase of the second mode contributes significantly to the seam wave signal if the dirt band lies near the centre of the seam. Interference with the first mode produces seam wave signals with irregular shapes and amplitudes. In practice, these irregularities might be responsible for poor processing results.

Furthermore, fault characteristics were investigated by means of the reflectivity and transmissivity curves. The throw, the dip angle of the fault plane and the impedance in a fault zone were varied and are discussed with respect to fault detection. Comparison of the curves exhibits ambiguities which might be reduced by supplementing the field data by broad-band recordings and data acquisition on profile points in the surrounding rocks.

Key words: Finite difference method – Love seam waves – Wave guide – Dirt band – Coal seam discontinuities – Faults

Introduction

Mechanized longwall coal mining is economical only for exploiting regions of hard coal in which the seam is not disturbed by extensive dirt bands or faults. In fact, these disturbances occur frequently in European coal fields. Their detection provides an estimate of the productivity of the coal field during mine planning. So, a capital-intensive interruption of the coal production can be avoided.

Offprint requests to: C. Kerner

A powerful geophysical detection method is in-seam seismology (Arnetzl and Klinge, 1982; Brentrup, 1979; Buchanan, 1983; Dresen et al., 1985; Millahn, 1980; Rüter and Schepers, 1979). As coal has lower body-wave velocities compared with those of the cheek – i.e. the rock above and below the seam – channel waves are generated by a seismic source inserted into the coal (Krey, 1963). These channel waves are guided within the seam (seam waves) and are recorded at distances as far as 1.5 km from the source (Arnetzl, 1971). Until now, underground surveys have concentrated on Love seam waves.

The in-seam seismic method is well established. However, the manifold effects of the layering of a seam (i.e. dirt band embeddings), or the layering of the cheek (i.e. root clay layers), for example, can lead to an erroneous interpretation of the underground data. On the other hand, more detailed information on the characteristics of a discontinuity (fault, erosion, fold, etc.) or the geometry (fault offset, length of the eroded region in the seam, etc.) is required.

A better understanding of the physical effects of the geological disturbances on the transmission and reflection of seam waves is one way to improve data interpretation regarding target recognition, location and identification. For this purpose, seismic modelling with a layer matrix method was introduced by Räder et al. (1985). Asten et al. (1984) and Edwards et al. (1985) used a finite element method for their studies on seam waves. In this paper, similar to Korn and Stöckl (1982), we have numerically simulated Love seam wave propagation with a finite difference (FD) method. Amplitude and dispersion curves are compared with theoretical values calculated with the layer matrix method. Two topics are studied:

– the effect of rock and/or soil embeddings in the seam (dirt bed or dirt band) on Love seam wave propagation
– the effect of fault characteristics on the reflection and transmission of Love seam waves.

Layered seams have previously been investigated by Räder et al. (1985). From dispersion curves and amplitude-depth distributions these authors concluded that, for dirt band embeddings, wave groups of higher modes will occur in addition to the Airy phase of the first mode. Here, we investigate the effect of interfering modes. Vertical faults have been analysed by Korn and Stöckl (1982). We extend their work and study dipping fault planes and fault zones of finite width which interrupt the continuity of the coal layer.

Methods of computation

Finite difference method

In Cartesian coordinates, the two-dimensional equation of motion for an *SH* wave propagating in heterogeneous media is

$$\frac{\partial^2 v}{\partial t^2} = 1/\rho \left[\frac{\partial}{\partial x} \left(\mu \frac{\partial v}{\partial x} \right) + \frac{\partial}{\partial z} \left(\mu \frac{\partial v}{\partial z} \right) \right], \tag{1}$$

where x and z are the two components of the radius vector, $v(x, z, t)$ is the displacement, $\rho(x, z)$ is the density and $\mu(x, z)$ is the shear modulus.

This equation can be solved numerically by applying a finite difference method: discretization of the medium by a rectangular grid of equal spacing Δx and Δz and time discretization by time steps Δt yield a sampling of the continuous functions v, μ and ρ. The following notation is used:

$$\begin{aligned} &v(m \cdot \Delta x, n \cdot \Delta z, l \cdot \Delta t) = v^l_{m,n} \\ &\rho(m \cdot \Delta x, n \cdot \Delta z) = \rho_{m,n} \\ &\mu(m \cdot \Delta x, n \cdot \Delta z) = \mu_{m,n}. \end{aligned} \tag{2}$$

Standard central differences with a truncation error of second-order (Boore, 1970) are employed to approximate the partial differentials in the equation of motion. The following recursion formula for the calculation of $v^{l+1}_{m,n}$, the displacement in the grid point m, n at the time $l+1$, is obtained (Boore, 1972):

$$\begin{aligned} v^{l+1}_{m,n} = {} & 2v^l_{m,n} - v^{l-1}_{m,n} + [\Delta t^2/\Delta x^2 [\mu_E (v^l_{m+1,n} - v^l_{m,n}) \\ & - \mu_W (v^l_{m,n} - v^l_{m-1,n})] \\ & + \Delta t^2/\Delta z^2 [\mu_S (v^l_{m,n+1} - v^l_{m,n}) \\ & - \mu_N (v^l_{m,n} - v^l_{m,n-1})]]/\rho_{m,n}, \end{aligned}$$

where: (3)

$$\mu_E = 1/2(\mu_{m+1,n} + \mu_{m,n}) \qquad \mu_N = 1/2(\mu_{m,n} + \mu_{m,n-1})$$

$$\mu_W = 1/2(\mu_{m-1,n} + \mu_{m,n}) \qquad \mu_S = 1/2(\mu_{m,n} + \mu_{m,n+1}).$$

At the start of the recursion, in accordance with an arbitrary source signal, the displacements are prescribed at a given source point.

Numerical stability of the explicit scheme in Eq. (3) is guaranteed if the relation $\Delta t = h_{\min}/(\beta_{\max} \cdot \sqrt{2})$ between the time step Δt, the minimum grid spacing $h_{\min} = \mathrm{MIN}(\Delta x, \Delta z)$ and the maximum shear wave velocity in the model $\beta_{\max} = \mathrm{MAX}[(\mu_{m,n}/\rho_{m,n})^{-1/2}]$, is used. Artificial reflections from the edges of the model are sufficiently suppressed by applying the boundary conditions suggested by Reynolds (1978). Grid dispersion is reduced if the smallest predominant wavelength λ_H, defined by the upper frequency of half the maximum amplitude in the source spectrum, corresponds to ten or more grid spacings $h_{\max} = \mathrm{MAX}(\Delta x, \Delta z)$ (Alford et al., 1974).

A large computational effort is needed for FD simulations even on fast machines. This limits the use of the method to problems where the wave propagation over distances of only some few wavelengths is to be investigated. In particular, seam waves can be studied by FD as these waves propagate in the coal and the neighbouring rock. Thus, only a relatively small part of the geological structure has to be modelled. Nevertheless, 250 grid points in the x-direction and 100 grid points in the z-direction are necessary for even a simple structure. This means that at each time step $250 \times 100 = 25{,}000$ 'new' displacements have to be calculated. If the wave needs 2,000 time steps to travel through the model, the above recursion formula must be solved 50 million times: CPU-times of around half an hour are required for the computation of such a model on a conventional computer like the Cyber 175.

A remarkable improvement in the speed of the FD program by a factor of 35 was obtained on a Cyber 205 vector machine. Computations on the Cyber 205 demand a coding of the algorithm in 'vector-FORTRAN'. It is the non-recursive portion of the FD algorithm, i.e. the iteration over the grid points, that is performed by parallel vector operations (Kerner, 1985).

Amplitude and dispersion analysis

An analysis of amplitudes and phase-velocity dispersion of the Love seam waves was carried out. In the case of a fault, the maximum displacement amplitudes of the reflected and transmitted waves (A_R, A_T) are determined. The values are normalized by the amplitude of the incident seam wave. Their representation as a function of the parameters of the fault – e.g. the throw – gives concise information about the effect of the parameters on the detectability of the fault.

More detailed information is drawn from a spectral amplitude analysis of the reflected and transmitted seam waves. We analysed the waves recorded in the centre of the seam on both sides of the fault and normalized the spectra by the amplitude spectrum of the incident Love seam wave. Thus, we remove the influence of the source signal and the filtering effects of the layering. Korn and Stöckl (1982) called the normalized spectrum of the reflected wave $S_R(f)$ the 'reflectivity' and that of the transmitted wave $S_T(f)$ the 'transmissivity', where f is the frequency. In the case of a seam interlayered with a dirt band, we are interested in the mode identification of the waves propagating in each of the layers. This is done by analysing the phase velocities and comparing the results with theoretical dispersion curves. A phase difference method was used for the dispersion analysis (Dziewonski and Hales, 1972).

From the amplitude-depth curves $V(f, z)$, the transfer properties of the layering with respect to seam waves recorded in the coal are deduced. In a sequence rock-coal-rock, the ratio of the signal amplitudes recorded within the seam to those recorded in the rock grows with increasing frequency. This implies a high-pass filtering effect in the coal. Two quantities are used to describe the filtering effect.

For each frequency, the kinetic energy density averaged over one period can be determined for a layer of thickness d and density ρ_l with the formula

$$E(f) = -1/4(2\pi f)^2 \rho_l \int_{-d/2}^{+d/2} V^2(f, z)\, dz. \tag{4}$$

Normalization of the energy density in the layer by the total energy density in all layers, gives values of the 'relative energy'

$$E_R(f) = \rho_l \int_{-d/2}^{+d/2} V^2(f, z)\, dz \Big/ \int_{-\infty}^{+\infty} \rho(z) V^2(f, z)\, dz. \tag{5}$$

For each frequency, the energy transport in any given layer is estimated with respect to the total energy: $E_R = 1$ means that the total energy transport is restricted to the layer (e.g. the coal layer), $E_R = 0$ indicates that the total energy is transported outside the layer (Dresen and Freystätter, 1976). The relative energy has been determined from amplitude-depth distributions calculated with the layer matrix method.

Instead of the relative energy, the 'relative amplitudes' can be evaluated from the formula

$$V_R(f) = \int_{-d/2}^{+d/2} V(f,z)\,dz \Big/ \int_{-\infty}^{+\infty} V(f,z)\,dz. \qquad (6)$$

Relative amplitudes are determined from amplitude-depth distributions extracted from synthetic seismograms. They provide similar information to that given by the relative energies. They were calculated in the case of seismogram analysis to avoid the use of information concerning the layer densities which are not known in real situations.

Models

Figure 1 shows sketches of the models under investigation. They represent vertical sections through earth layers and through tectonic structures. The characteristics and parameters of each model are specified in Table 1. Mean values of shear-wave velocities and densities in different rock and coal layers known from field surveys are assumed in all models (Table 2). As usual in the in-seam seismic technique, the source is positioned in the middle of the thickest coal layer.

Four models are chosen to examine the influence of dirt bands (Fig. 1a). The seam, consisting of two coal layers (c, c_s) and one dirt band (d), is embedded in a homogeneous rock material (r). Since, in nature, the dirt band material is often the same as the rock material, we choose the same velocities and densities in both the rock and dirt bands. In models Db(1) and Db(2) (Table 1), the dirt band separates the seam into two coal layers with equal thickness. In view of the results of Räder et al. (1985), we choose the thickness of the dirt band so that it significantly affects the wave propagation. This means that the dirt band thickness relative to the seam thickness has to take on values in the range from 0.05 to 0.33 (Kerner, 1984). Räder et al. (1985) pointed out that, outside this range, the dirt band is either so thin that it scarcely affects the seam wave or the dirt band causes a separation between the coal layers so large that the seam wave is guided mainly in the source-containing coal layer. In models Dp(1) and Dp(2), the position of the dirt band is varied, yielding two characteristic ratios of coal layer thicknesses.

Two types of fault models are designed for studying the effect of various fault parameters on the seam wave propagation. A fault where the degree of throw is several times greater than the seam thickness was realized by terminating the seam at the fault (seam end, Fig. 1b). Investigation of this fault type is basic because there are no effects from that part of the seam behind the fault. In the second model type, the throw of the fault is less than twice the seam thickness. Hence, the part of the coal layer behind the fault is modelled as well (Fig. 1c–e).

In models Ez(1)–Ez(4), the fault plane is vertical. A fault zone was constructed and the impedance of the material in the fault zone was varied. Choosing the same elastic parameters in the fault zone as in the rock, in the case of model Ez(1), means that there is no fault zone at all. In model Ez(2), the elastic parameters are chosen so that the impedance in the fault zone is lower than in the coal and rock. In reality, this can be interpreted as disaggregation of the rock material in the zone by fracturing. Choosing an impedance in the fault zone of Ez(4) higher than the impedances in the coal and rock, we model a consolidation of the material in the fault zone. In model Ez(3), an intermediate value is chosen for the impedance in the fault zone. In all the models Ez, the thickness of the fault zone is about 10% of the seam thickness, which means a two-way travel distance of less than a quarter wavelength for waves propagating horizontally through the zone. In models Ed(1)–Ed(3), three different values γ less than 90° are chosen for the dip angle of the oblique fault plane.

In models Fs(1)–Fs(5), the value of the throw relative to the seam thickness is varied. In models Fz, a fault zone is constructed using the same impedances as in the case of models Ez. For all Fz models, the throw is about half the seam thickness. While the fault plane is vertical in models Fs and Fz, in models Fd and Fu the fault plane dips. Models Fd contain down-dipping faults and models Fu contain up-dipping faults. The same angles as in the seam end models Ed are chosen. A constant throw of one seam thickness is used.

The FD grid consists of 250 points in the x-direction and 100 points in z-direction. In the fault models, the thickness of the coal layer is represented by 9 grid points. A grid spacing of 0.4 m in the x- and z-directions is chosen.

The number of grid points for the seam has to be increased to model an interlayering of the coal. We used 15 grid points in the vertical direction for the source-containing coal layer in all dirt band models except Dp(1). In the latter model, 11 grid points represent the seam. Grid

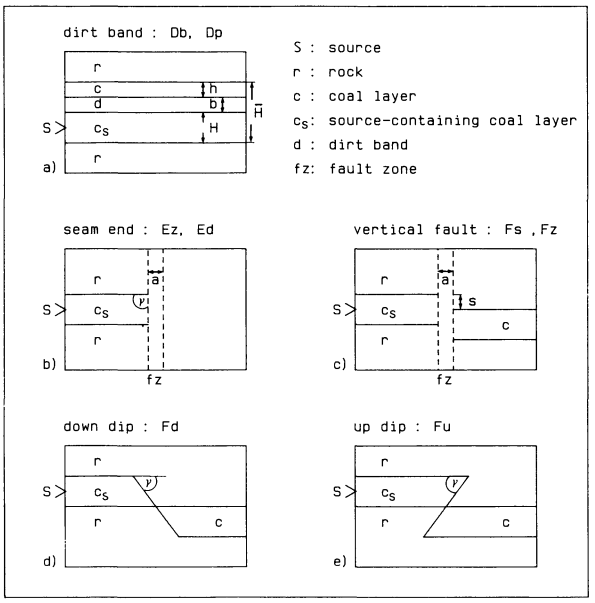

Fig. 1a–e. Sketches of the models. *H:* thickness of the source-containing coal layer, *h:* thickness of the coal layer without source in the dirt band models, *b:* thickness of the dirt band, $\bar{H}$: thickness of the total seam in the dirt band models, *s:* throw, *a:* width of the fault zone, γ: dip angle of the fault plane

Table 1. Model parameters

Model type	Characteristic	Variable parameters	Constant parameters
Db	Variation of the thickness of the dirt band	1: $b/\bar{H}=0.14$ 2: $b/\bar{H}=0.27$	$h/H=1$
Dp	Variation of the position of the dirt band	1: $h/H=0.82$ 2: $h/H=0.33$	$b/\bar{H}=0.2$
Ez	Variation of the impedance in a fault zone	1: $I_{fz}=6.0\ 10^5$ g/(cm^{2}s) 2: $I_{fz}=0.9\ 10^5$ g/(cm^{2}s) 3: $I_{fz}=3.5\ 10^5$ g/(cm^{2}s) 4: $I_{fz}=8.0\ 10^5$ g/(cm^{2}s)	$\gamma=90°$ $a/H=0.11$ $s/H\gg 1$
Ed	Variation of the dip angle of the fault plane	1: $\gamma=27°$ 2: $\gamma=45°$ 3: $\gamma=63°$	$a/H=0$ $s/H\gg 1$
Fs	Variation of the offset at the fault	1: $s/H=0.33$ 2: $s/H=0.56$ 3: $s/H=0.78$ 4: $s/H=1.00$ 5: $s/H=1.67$	$a/H=0$ $\gamma=90°$
Fz	Variation of the impedance in a fault zone	1: $I_{fz}=0.9\ 10^5$ g/(cm^{2}s) 2: $I_{fz}=3.5\ 10^5$ g/(cm^{2}s) 3: $I_{fz}=6.0\ 10^5$ g/(cm^{2}s) 4: $I_{fz}=8.0\ 10^5$ g/(cm^{2}s)	$\gamma=90°$ $s/H=0.56$ $a/H=0.11$
Fd	Down-dipping fault: variation of the dip angle of the fault plane	1: $\gamma=27°$ 2: $\gamma=45°$ 3: $\gamma=63°$	$s/H=1.00$
Fu	Up-dipping fault: variation of the dip angle of the fault plane	1: $\gamma=27°$ 2: $\gamma=45°$ 3: $\gamma=63°$	$s/H=1.00$

Table 2. Elastic parameters

	Shear-wave velocity (km/s)	Density (g/cm^3)	Impedance [10^5 g/(cm^{2}s)]
Rock (dirt band)	2.3	2.6	6.0
Coal	1.2	1.4	1.7

spacings of 0.2 m in the z-direction and 0.4 m in the x direction are chosen.

We used Küpper's wavelets (Küpper, 1958) as source signals, with two amplitude extrema. The duration of the wavelet is chosen such that the spectral amplitudes of the generated seam waves are higher than 5% of the maximum spectral amplitude in a range from 200 to 1400 Hz·m on the $f\cdot H$ scale (f: frequency; H: thickness of the source-containing coal layer. We use this scale, instead of the frequency scale, to make the results independent of the thicknesses of the layers chosen in the models). The maximum spectral amplitude occurs at 800 Hz·m (fault models), or close to this value (dirt band models). At this value, the group-velocity dispersion curve of the first mode takes on its minimum value. So, the generated seam wave contains the Airy phase of the first mode which is of special interest in the field survey due to its low amplitude decrease with distance.

For all models except Dp(1), the numerical errors from grid dispersion are less than 5% for the amplitudes and less than 3.5% for the phase velocities in the $f\cdot H$-range below 1400 Hz·m. The same holds for the model Dp(1), below 1100 Hz·m. Interference of the signals with residual artificial reflections from the edges of the model can cause errors of a maximum of 5% in the phase-velocity analysis.

Seams interlayered with dirt bands

Bands of different thicknesses

The seismogram sections displayed in Fig. 2 are calculated for profiles running vertically through the layer sequences in models Db(1) and Db(2). The layer interfaces are marked on the vertical axis.

The seismogram examples show that one part of the seam wave, occurring in both sections in the time interval from about 36 to 90 ms, is guided within the total seam. Amplitudes of this part of the seam wave are high in both the coal layers and in the dirt band. Another part of the seam wave, occurring in the time interval from about 90 to 108 ms, exhibits high amplitudes only within the coal layers while the amplitudes of the phases recorded within the dirt band are nearly zero. For this part of the seam wave, only the coal layers act as wave guides.

In addition to this information, which was also obtained from the dispersion curves and the amplitude-depth distributions (Räder et al., 1985), the seismograms recorded in the coal show that both parts of the seam wave occur simultaneously, forming an extremely long seam wave signal. The two wave parts do not form a continuous wavelet as would be expected if both parts belong to the same (first) mode, but there are gaps with low amplitudes at times of

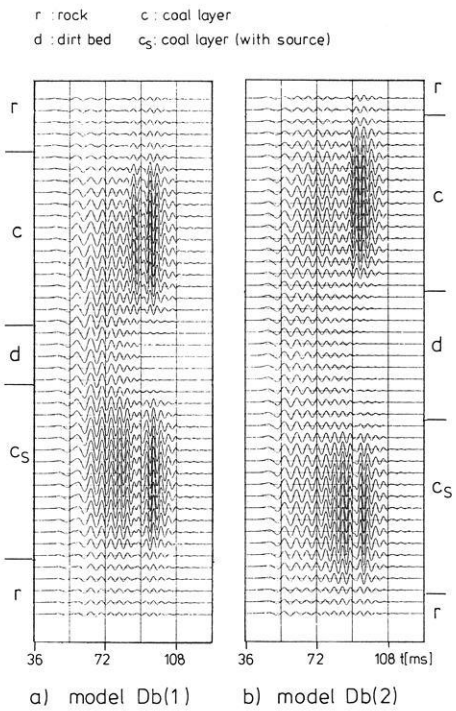

Fig. 2a and b. Seismogram sections calculated for vertical profiles in the models Db. Distance of the profiles from the source position: $x/H = 30.7$

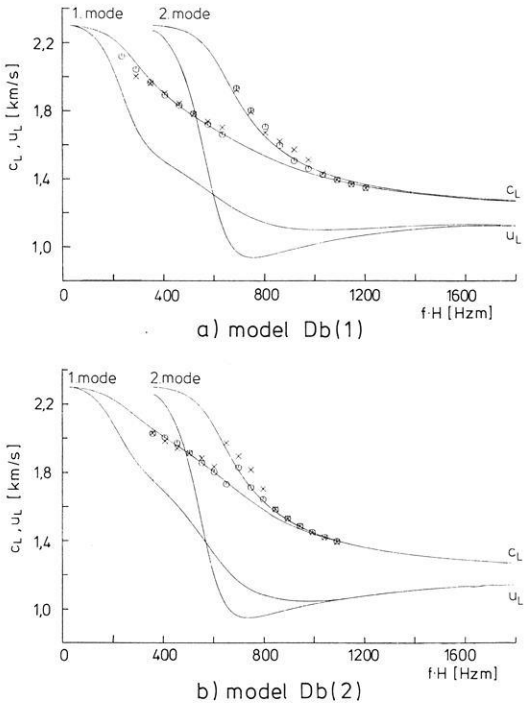

Fig. 3a and b. Phase(c_L)- and group(u_L)-velocity dispersion curves of the first and second mode and results from the phase-velocity analysis of the seam waves propagating in the source-containing coal layer (*crosses*) and in the coal layer without source (*circles*)

about 90 ms (Fig. 2a: refer to the signals in c and c_s; Fig. 2b: refer to the signals in c_s).

Phase-velocity analysis was carried out to determine the modes with which the seam wave phases have to be associated. Seismogram sections calculated for horizontal profiles positioned in the centre of either of the two coal layers were analysed. For the models Db, the results together with the phase- and group-velocity dispersion curves of the first and the second mode are displayed in Fig. 3.

Both graphs (Fig. 3a and b) show that the low-frequency part of the seam wave propagating in the total seam belongs to the first mode. The results agree with the theoretical curve in the $f \cdot H$-range from 300 to 650 Hz·m, where an indentation characterizes the group-velocity dispersion curves of the first mode. However, the high frequency parts of the seam wave propagating within the coal layers in Db(1) and Db(2) belong to the Airy phase of the second mode in the $f \cdot H$-range from 650 to 900 Hz·m. Above 900 Hz·m the phase velocities from the analysis correlate with the phase-velocity dispersion curves of both the first and the second mode.

The following should make plausible why the change from the first to the next higher mode occurs. From the amplitude-depth distributions (Räder et al., 1985), it is obvious that the source position in the centre of the coal layers is optimal for an excitation of either the first or the second mode in an $f \cdot H$-range from about 600 to 1200 Hz·m. Maximum amplitudes occur in this position. Kerner (1984) demonstrated that sharp group-velocity minima, i.e. steep descents in the vicinity of minima, yield a sharp impulse-like Airy phase signal with large amplitudes, while smooth minima yield less prominant Airy phase signals. Hence, it is obvious that in combination with optimal source conditions for generating both modes, the preferential excitation of the second mode is caused by the more pronounced group-velocity minimum of this mode, as apparent in Fig. 3.

For model Db(1), the relative energy versus $f \cdot H$ (Fig. 4) is plotted. The curves derived from the theoretical amplitude-depth distributions were computed for the first and second mode. They describe the portions of energy guided in each of the coal layers. As in the case of the simple layer sequence rock-coal-rock, the general trend of the curves indicates the high-pass filtering effect on the amplitudes of the seam wave phases guided in the coal layers as well as in the case of the layering with dirt band. The results from the analysis (Fig. 3a) agree with the information obtained from the energy distributions (Fig. 4). In the $f \cdot H$-range below 650 Hz·m, where the first mode dominates, the energy of the first mode is much higher than the energy of the second mode. In the range from 650 to 900 Hz·m, the curve of the relative energy determined for the second mode lies above the one calculated for the first mode. Above 900 Hz·m, both curves approach the maximal value of relative energy guided in each of the two coal layers ($E_R = 0.5$). This means that there is no preferential excitation of either of the two modes. Similar energy curves were obtained for model Db(2).

Curves of the relative amplitude distribution were calculated for the models Db from amplitudes extracted from the seismogram sections presented in Fig. 2. In contrast to the curves of relative energy, the curves for the relative amplitude exhibit effects which result from an overlapping of phases of the first and the second mode. The curves of relative amplitude depend specifically on the distance of the vertical profile from the source and the source position. The curves in Fig. 5 describe the dependence on $f \cdot H$ of the relative amplitudes of seam wave phases guided in the two coal layers. There are significant effects on the

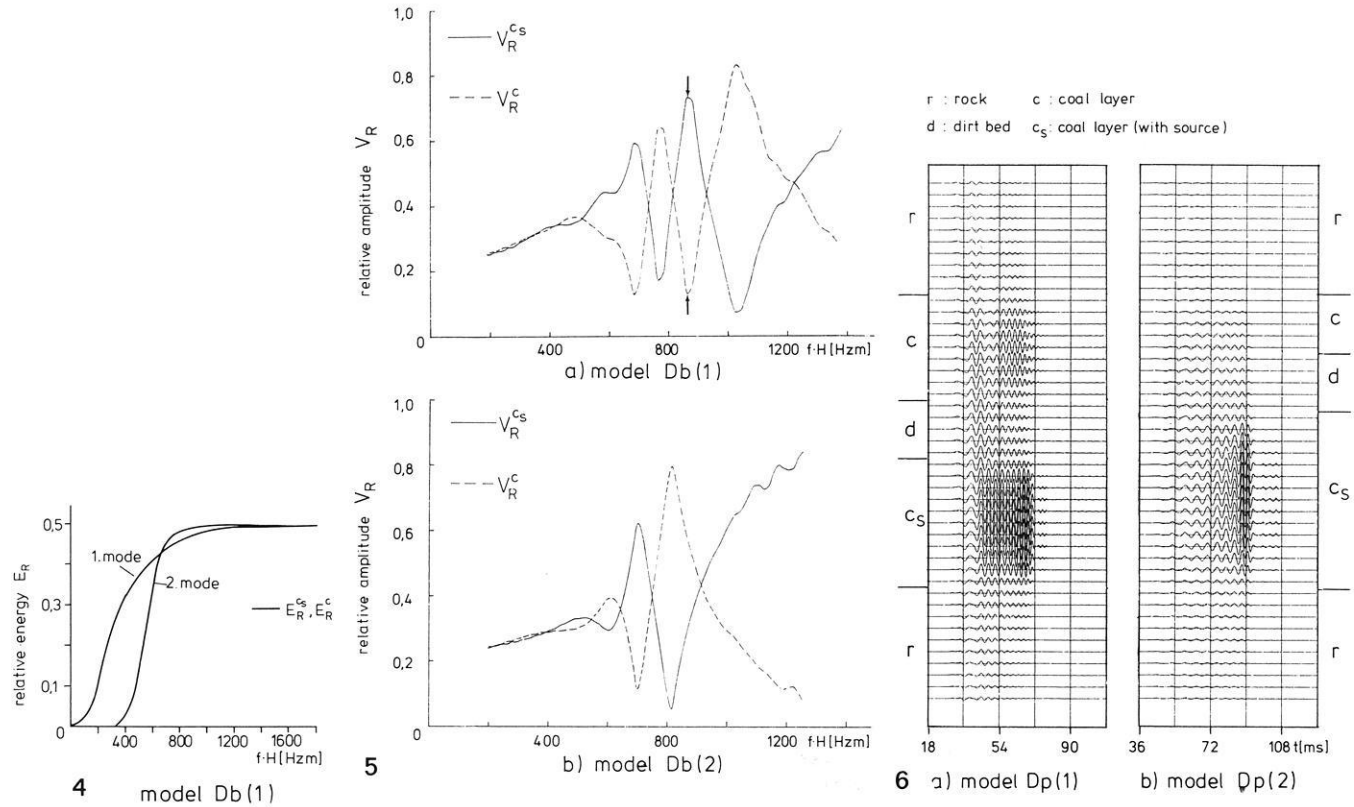

Fig. 4. Curves of the relative energy E_R for waves guided in the coal layers $c_s(E_R^{c_s})$ and $c(E_R^c)$ of the model Db(1). The curves are calculated for the first and second mode

Fig. 5a and b. Curves of the relative amplitude V_R for waves guided in the coal layers $c_s(V^{c_s}{}_R)$ and $c(V_R^c)$ of the models Db

Fig. 6a and b. Seismogram sections calculated for vertical profiles in the models Dp. Distance of the profiles from the source position: $x/H = 30.7$

amplitudes in the $f \cdot H$-range from 600 to 1200 Hz·m in the case of model Db(1) (Fig. 5a) and from 600 to 900 Hz·m in the case of model Db(2) (Fig. 5b). The oscillations in this range can be explained by constructive and destructive interference of seam wave phases of the first and second mode. The effect of the interference depends on the phase difference between waves of the first and the second mode due to different phase velocities and the signs of the amplitudes in the amplitude-depth distributions. For example, in Fig. 5a the maximum (arrow) at 850 Hz·m in the curve describing the relative amplitude in the source-containing coal layer (solid line) occurs because the interfering first and second mode are in phase (Fig. 6 in Räder et al., 1985). The equivalent minimum (arrow) at 850 Hz·m in the curve describing the relative amplitude in the other coal layer (dashed line) occurs because the two modes are 180° out of phase (Fig. 6 in Räder et al., 1985).

Summary 1

It was found that besides the seam wave propagating in the wave guide 'total seam' (which is associated with the first mode), it is not, as usually assumed in practice, the Airy phase of the first mode which propagates in the wave guides 'coal layers', but the Airy phase of the second mode. Interference of waves belonging to the two modes causes pronounced minima and maxima in the curves of relative amplitude. No significant effects which depend on the thickness of the dirt band are found.

Position of dirt band within the seam

The seismogram sections in Fig. 6 calculated for vertical profiles in the models Dp show that the seam wave propagation is significantly influenced by the position of the dirt band within the seam. In the case of Dp(1) (Fig. 6a), the two wave portions guided in the wave guides 'total seam' and 'coal layers' can be distinguished, but the amplitudes of the signals recorded in the coal layer without source are smaller than those recorded in the source-containing coal layer. In the case of Dp(2) (Fig. 6b), seam wave propagation is concentrated in the source-containing coal layer.

The dispersion curves and the results from the velocity analysis for the models Dp are depicted in Fig. 7. In the case of Dp(2) (Fig. 7b), only the first mode is excited with significant amplitudes. All phase velocities of the seam waves propagating in the source-containing coal layer, and most of the phase velocities of the seam waves propagating in the coal layer without source, coincide with the dispersion curve of the first mode. The amplitude of the Airy-phase signal is evanescent in the coal layer without source. Therefore, the high-frequency wave part which can be seen at the beginning of the seam wave signal (Fig. 6b at 54 ms)

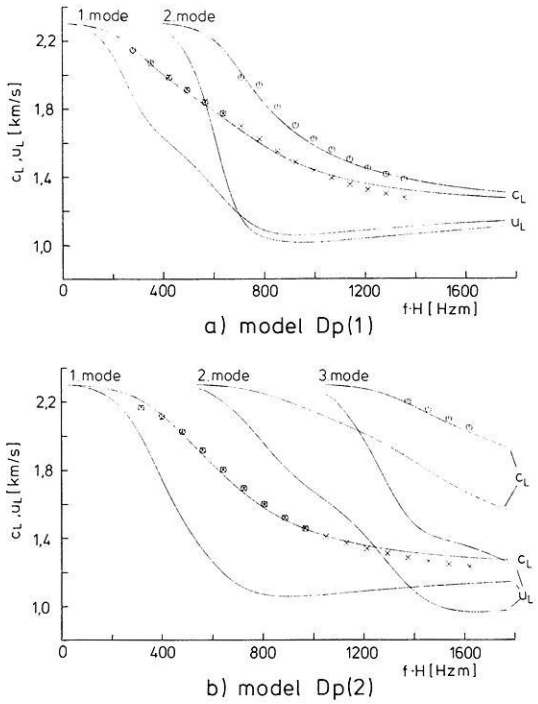

Fig. 7a and b. Phase(c_L)- and group(u_L)-velocity dispersion curves of the first and second mode and results from the phase-velocity analysis of the seam waves propagating in the source-containing coal layer (*crosses*) and in the coal layer without source (*circles*)

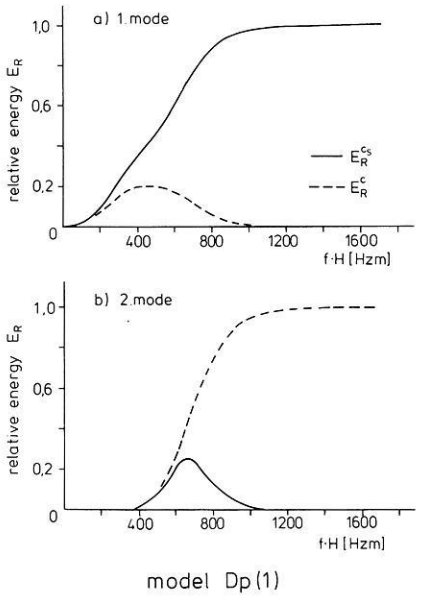

Fig. 8a and b. Curves of the relative energy E_R for waves guided in the coal layers $c_s(E_R^{cs})$ and $c(E_R^c)$ of the model Dp(1)

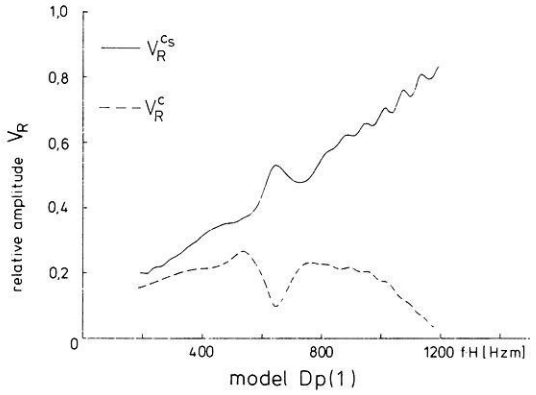

Fig. 9. Curves of the relative amplitude V_R for waves guided in the coal layers c_s (V_R^{cs}) and $c(V_R^c)$ of the model Dp(1)

was identified by the velocity analysis as belonging to the third mode (Fig. 7b).

In the case of model Dp(1), the results obtained for the seam wave propagating in the coal layer without source again show that the first mode is excited in the $f \cdot H$-range where the group-velocity dispersion curve has an indentation and that the Airy phase of the second mode is excited. In contrast to this finding, all phase velocities of the seam wave propagating in the source-containing coal layer coincide with the phase-velocity dispersion curve of the first mode.

The curves of relative energy in Fig. 8 explain the above results. The curve calculated for the first mode of the seam wave propagating in the source-containing coal layer (solid line in Fig. 8a) has the previously mentioned high-pass filter characteristic with values approaching the maximum value above 800 Hz·m. This means that nearly all of the wave energy of the first mode is guided in the source-containing coal layer. The relative energy curve belonging to the seam wave of the first mode propagating in the coal layer without source (dashed line in Fig. 8a) indicates that only in the $f \cdot H$-range around 400 Hz·m, where the indentation in the group-velocity dispersion curve occurs, is a small energy portion of the first mode guided within this coal layer. The results for the second mode are just the opposite (Fig. 8b). Only a small portion of wave energy of the low-frequency part of the second mode is guided within the source-containing coal layer, while the second mode is completely trapped within the coal layer without source if this mode is excited in the $f \cdot H$-range above 1000 Hz·m. As energy transport is confined to one coal layer, the effects of interference are not as pronounced as in the case of models Db. Only around 650 Hz·m do the curves of relative amplitude in Fig. 9 show weak oscillations resulting from overlapping of waves of the first and second mode.

Summary 2

The influence of higher modes decreases if the dirt band is not positioned in the centre of the seam. From a comparison of the group-velocity dispersion curves of all dirt band models investigated, it is concluded that for any given layer sequence the significance of higher modes can be deduced from the positions of the group-velocity minima on the $f \cdot H$ scale relative to each other and from the extent to which they are pronounced. Curves of relative energy are useful in this prognosis.

Seams interrupted by faults

Seam end

In Fig. 10, curves of the reflectivity calculated for models Ez are presented. The normalized maximum signal amplitudes of the reflected seam wave signals are listed in a table.

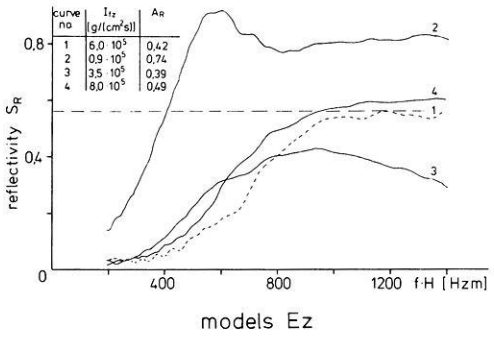

Fig. 10. Reflectivity S_R versus $f \cdot H$ calculated for the seam end models Ez containing fault zones. *Table:* Maximum signal amplitudes A_R of the reflected seam wave

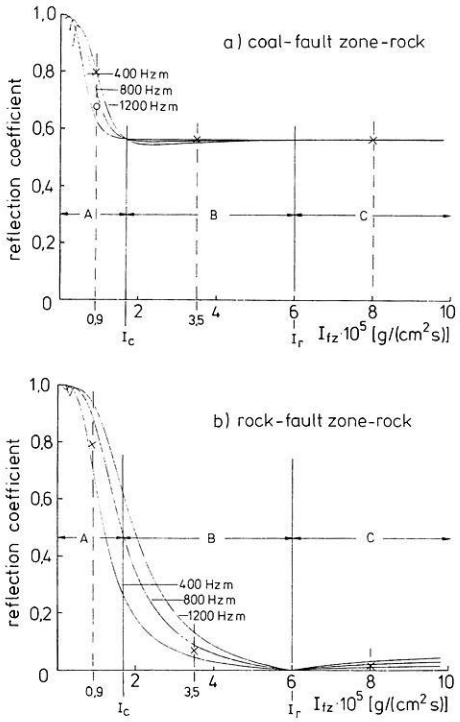

Fig. 11a and b. Reflection coefficient of the *SH* wave vertically incident on a thin layer (fault zone) versus the impedance of the layer I_{fz} (I_c: impedance of the coal, I_r: impedance of the rock)

These values correspond to the reflectivity values of the Airy phase of about 800 Hz·m.

The dashed curve in Fig. 10, calculated for model Ez(1) without a fault zone (Fig. 1), serves as a reference curve. From an approximation of this curve by an analytically calculated curve, Korn and Stöckl (1982) deduced that in the case of a simple vertical truncation of the seam (seam end) the reflectivity is mainly determined by two factors:

– The faults acts as a high-pass filter on the reflected seam wave. Accordingly, the reflectivity curve exhibits the characteristics of a high-pass filter curve.

– In the pass-band of the filter (>1000 Hz·m), the reflectivity approaches the reflection coefficient for normal incidence of the interface coal-rock. This value is equal to 0.56 in our models (horizontal line).

Comparison of the reflectivity curve (2) with the dashed curve shows that a zone of fractured rock material (disaggregation) at the fault produces a significant increase in the amplitudes of the reflected seam wave signal. For high frequencies ($f \cdot H > 800$ Hz·m), the reflectivity is about 0.8. A zone of consolidated rock material also produces an increase in the amplitudes, but the effect is less prominent. Above 800 Hz·m, the reflectivity curve (4) lies about 10% above the reference curve and approaches values of about 0.6. For an intermediate impedance, the reflectivity curve (3) lies below the reference curve for $f \cdot H > 800$ Hz·m. A maximum value of 0.43 occurs at 950 Hz·m. Below 800 Hz·m, all of the solid curves lie above the reference curve. Thus, there is a reduction of the high-pass filter effect of the fault if there is a fault zone. However, this effect is significant only for fractured zones.

To extend the results obtained by Korn and Stöckl (1982) to fault zones, we assume that at high frequencies the reflectivity is mainly determined by the reflection of the seam wave propagating in the coal layer. Therefore, the reflectivity values should approach the reflection coefficient for a plane *SH* wave reflected from the two interfaces of the fault zone, the coal-fault zone interface and the fault zone-rock interface. Furthermore, it seems reasonable to suppose that the reduction of the high-pass filter effect of the fault is caused by the reflection of the low-frequency seam wave propagating in the rock. For these waves, the reflection coefficients for an *SH* wave reflected from the interfaces rock-fault zone and fault zone-rock are relevant.

We have calculated reflection coefficients for a thin layer surrounded by two half-spaces with the layer matrix method (Fertig, 1982). The half-spaces are taken to have the elastic parameters of the coal and the rock, respectively, and the thin layer is taken to have the thickness of the fault zone. Figure 11 shows the results for the sequences coal-fault zone-rock (Fig. 11a) and rock-fault zone-rock (Fig. 11b) as functions of the impedance of the fault zone. The reflection coefficient resulting from interference of the reflections from the two interfaces of the thin layer is complex-valued and depends on frequency. We calculated the amount of the reflection coefficient for three frequencies, 400, 800 and 1200 Hz·m. In the further interpretation we omit the relative minima occurring for small impedance values. These minima are due to destructive interference of the double reflection.

Figure 11a shows that only in the range A, for impedances smaller than those of the coal, does the reflection coefficient of the *SH* wave reflected from the fault zone (thin layer) exceed the reflection coefficient of 0.56 for a reflection at the interface coal-rock. The reflection coefficient is nearly constant and approaches this value in the ranges B and C, for impedances between those of the rock and coal, and impedances larger than that of the rock, respectively. In addition, Fig. 11a reveals that only for the disaggregation is there a distinct dependence of the reflection coefficient on the frequency. Comparison of the reflection coefficients (crosses in Fig. 11a) with the reflectivity values above 1000 Hz·m (Fig. 10) shows that indeed the reflectivity in this $f \cdot H$-range is mainly determined by the reflection coefficient in the disaggregation case and the consolidation case. For the intermediate impedance, the reflection coefficients can not explain the decrease of the reflectivity values above 1000 Hz·m. Although Korn and Stöckl (1982) concluded that diffractions generated at the corners of the seam end are unimportant for the reflectivity, we

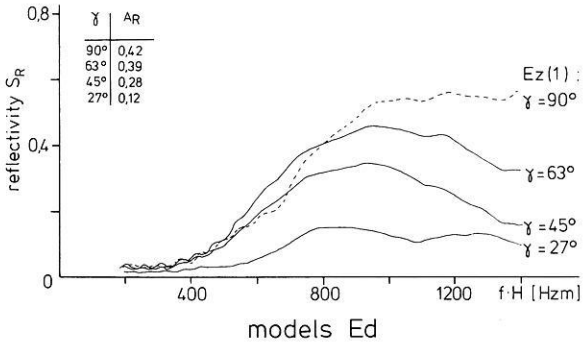

Fig. 12. Reflectivity S_R versus $f \cdot H$ calculated for the models Ed containing truncated seams (seam end) with dipping fault planes
Table: Maximum signal amplitudes A_R of the reflected seam wave

think that in the case of the fault zone, especially in the range B, diffraction phenomena are responsible for details, such as the one mentioned, in the reflectivity curves.

From amplitude calculations (Kerner, 1984), we know that the effects from the reflected seam wave portions propagating in the rock are strongest in the $f \cdot H$-range near 600 Hz·m. In this range, the seam wave exhibits amplitudes of comparable size in both coal and rock. Figure 1b shows that for $I_{fz} = 0.9 \times 10^5$ g/(cm^{2}s), the reflection coefficient is about 0.8 at 600 Hz·m (cross). As the wave portion in the seam is also reflected with similar reflection coefficients ($\cong 0.7$, circle in Fig. 11a), this explains the behaviour of the reflectivity curve from 300 to 800 Hz·m (Fig. 10) in the disaggregation case. At 600 Hz·m, a maximum value even occurs.

For $I_{fz} = 3.5 \times 10^5$ g/(cm^{2}s) and 8.0×10^5 g/(cm^{2}s), the reflection coefficients are 0.07 and 0.01, respectively (crosses). These small values cannot completely explain the actual reflectivity values which, for example, are nearly twice as large as the value in the reference curve at 600 Hz·m. In this low $f \cdot H$-range, phase differences between the reflected wave propagating in the rock and the reflected wave propagating in the coal might be responsible for these fine details, besides diffractions. We found phase differences of about $\pi/2$ in the latter two cases. This value changes only little with frequency. For the disaggregation, the phase differences are smaller than $\pi/4$ in the $f \cdot H$-range around 600 Hz·m.

Figure 12 shows the reflectivity curves calculated for the models Ed with dipping fault plane. The reflectivity curve determined for the seam end with a vertical fault plane serves as a reference curve. It can be seen that decreasing the dip angle of the oblique fault plane produces a decrease of the maximum value in the reflectivity curve. The diminution of the reflectivity values above 950 Hz·m for $\gamma = 63°$ and $\gamma = 45°$ indicates a reduced high-pass filter effect.

An attempt to explain these reflectivity curves by means of the reflection coefficients, which are dependent on the angle of incidence, failed not only when we considered the reflection of the entire seam wave by analogy with the reflection of a plane *SH* wave – as done in the case of the seam end with vertical fault plane – but also when we considered the reflection of single phases of the seam waves. This is due to the more complex wave propagation processes at an oblique fault plane as compared to a vertical fault plane.

With the help of the seismogram sections plotted in Fig. 13, we will try to elucidate these processes. For the seam end model with vertical fault plane and for the seam end model with the 27°-dipping fault plane, seismograms were calculated for points lying on a rectangular profile surrounding the seam end. The seismograms are normalized by the maximum amplitude in the sections. The seismograms recorded in the seam are excluded from this normalization because the maximum signal amplitudes of the direct seam waves (D) are about ten times larger than the amplitudes used for the normalization.

In the seismogram sections, it can be seen that the low-frequency portion of the direct seam wave (D), which is incident on the seam end, propagates into the rock region adjacent to the seam end (T). Calculations of the transmissivity show that this transmitted wave is hardly influenced by the obliqueness of the fault plane. In particular, the deficit of reflected wave energy in the high-frequency range above 800 Hz·m, in the case of the oblique fault plane (Fig. 12), cannot be explained by an increased transmission into this region. However, the sections exhibit high-frequency wave phases transmitted into the rock (ellipses). In the case of the vertical fault plane (Fig. 13a), these wave phases are interpreted as diffractions from the corners at the seam end. The waves exhibit higher amplitudes in the case of the oblique fault plane (Fig. 13b). This is caused by an additional scattering of refracted waves in all directions, occurring when the high-frequency wave portions are multiply reflected in the region of the fault dip.

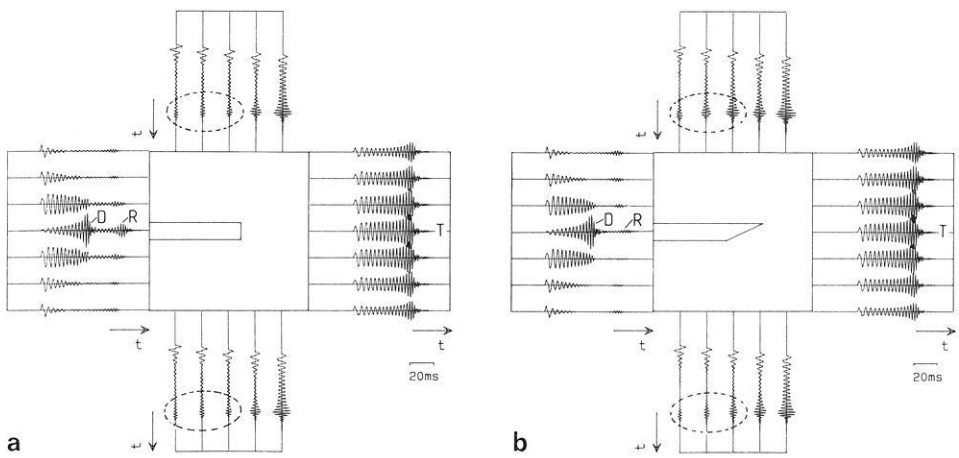

Fig. 13a and b. Seismogram sections calculated for a rectangular profile surrounding the seam end in the models **a** Ez(1) and **b** Ed(1) (D: direct seam wave, R: reflected seam wave, T: transmitted wave, *ellipses* contain transmitted waves scattered backwards)

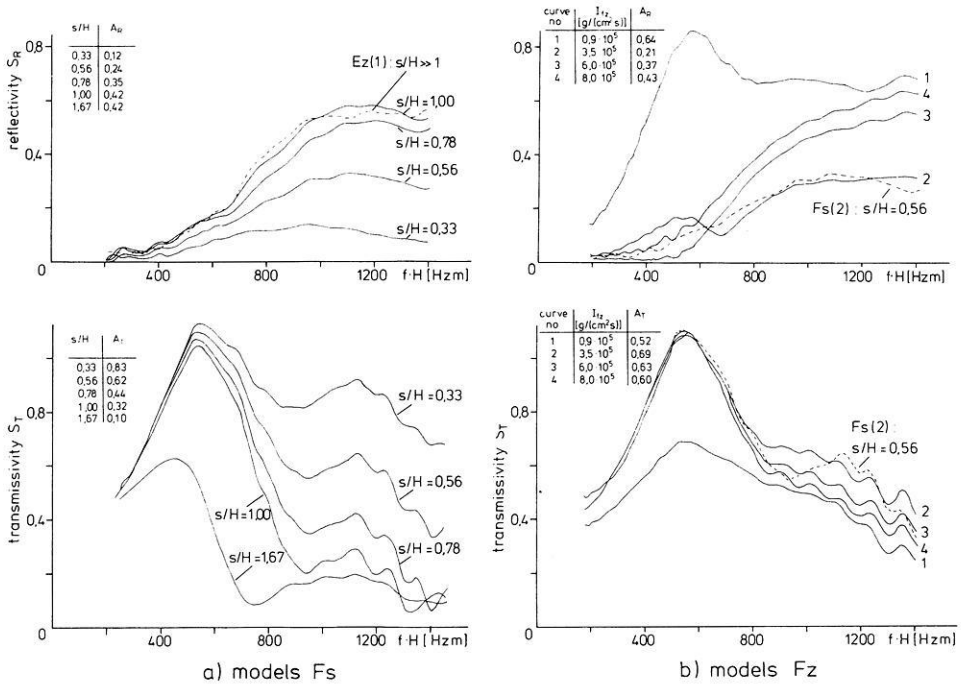

Fig. 14a and b. Reflectivity S_R and transmissivity S_T versus $f \cdot H$ calculated for **a** the models Fs containing faults with differing throws and for **b** the models Fz containing faults with fault zones *Tables:* Maximum signal amplitudes A_R and A_T of the reflected and transmitted seam waves

Summary 3

Only in the case of the disaggregation in the fault zone, is there a significant increase in the amplitude of the reflected seam wave signal compared with the amplitude in the case of the simple fault without a fault zone. The amplitude of the seam wave reflected by a disaggregation zone can be estimated by calculating reflection coefficients.

A dipping fault plane leads to a decrease in the amplitudes of the reflections. The high-frequency portion of the seam wave, especially, is scattered by the dipping fault plane.

Fault throw less/equal one seam thickness

The reflectivity curves for a seam with offset (Fig. 14a, top) exhibit a similar high-pass filter characteristic as does the reflectivity curve in the case of the truncated seam (dashed curve). The throw does not influence the amount of the reflectivity very much below $f \cdot H$ values of 650 Hz·m. Above this value, the reflectivity becomes significantly lower if the throw decreases below one seam thickness. For example, if the throw is one-third of the seam thickness, the amplitude of the reflection is 12% of that of the incident seam wave (refer to the upper table in Fig. 12a). No significant differences among the curves occur if the throw exceeds one seam thickness.

For the transmitted seam wave, the fault acts as a low-pass filter. Therefore, the transmissivity curves (Fig. 14a, bottom) exhibit a maximum at about 500 Hz·m. Below 800 Hz·m, the throw only produces minor differences among the transmissivity curves if the throw is less than or equal to one seam thickness. For the throw exceeding one seam thickness ($s/H = 1.67$), the maximum value of the transmissivity is halved, indicating low amplitudes of the transmitted seam wave for low frequencies. Due to the high-pass filter effect of the layering, the transmissivity values in the $f \cdot H$-range from 800 to 1400 Hz·m determine the maximum amplitude of the transmitted seam wave. In this range, the curves are characterized by a relative maximum at about 1100 Hz·m. The transmissivity is significantly dependent on the throw even for offsets less than one seam thickness (refer also to the amplitude values in the table).

Figure 14b shows the effects of the fault zone for a fault with a throw of about half a seam thickness. Inspection of the reflectivity curves (top) shows that all curves (1, 3, 4), except the one calculated for the intermediate impedance in the fault zone (2), lie significantly above the reference curve (dashed curve) calculated for the fault without any fault zone. Thus, both a zone with fractured rock material and a zone with consolidated rock material produce an increase in the amplitude of the reflected seam wave. The comparison of the respective signal amplitudes (table) confirms this result. The effect is explained by the fact that the reflection process at the fault is not restricted to the seam wave portions propagating at the level in the seam where the coal-rock interface occurs (Korn and Stöckl, 1982), as is the case at the simple fault with a throw less than one seam thickness, but is extended to the whole seam wave propagating in both coal and rock. In the case of the intermediate impedance in the fault zone, the reflectivity curve (2) closely follows the reference curve.

Inspection of the transmissivity curves (Fig. 14b, bottom) and a comparison of the amplitudes in the respective table show that there are no significant effects of the fault zone on the transmitted seam wave.

The reflectivity and transmissivity curves in Fig. 15 and the signal amplitudes in the tables show the effects from an oblique fault plane. The reflectivity curves calculated for the models Fd – which contain a down-dipping fault – (Fig. 15a, top) exhibit the same trends as already discussed for the respective seam end models (Ed). Although these reflectivity curves lie slightly ($\simeq 0.02$) above the respective curves (Fig. 12) above 800 Hz·m, the signal amplitudes of the reflected waves (table) are slightly smaller than

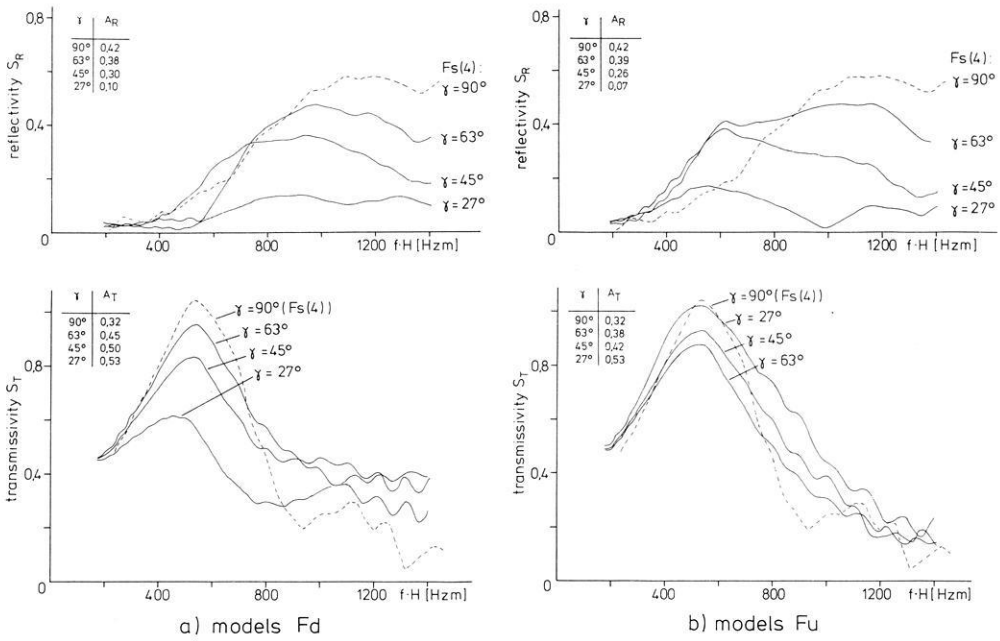

Fig. 15a and b. Reflectivity S_R and transmissivity S_T versus $f \cdot H$ calculated for **a** the models Fd containing faults with down-dipping fault planes and **b** for the models Fu containing faults with up-dipping fault planes
Tables: Maximum signal amplitudes A_R and A_T of the reflected and transmitted seam waves

those obtained for the models Ed. Comparison of the reflectivity curves calculated for the models Fu – which contain an up-dipping fault – (Fig. 15b, top) with the reflectivity curves for the models Fd shows that high reflectivity values occur in the range of low $f \cdot H$ values near 600 Hz·m. Above this value, the curves obtained for models Fd and Fu are similar but the reflectivity values are about 0.06 lower in the latter case. The signal amplitudes (table) are hardly affected by these differences.

The transmissivity curves for models Fu and Fd (Fig. 15a, b, bottom) indicate that the transmission of the high-frequency seam wave portion is favoured by the obliquity of the fault plane. The curves lie above the respective reference curve (dashed curve) for $f \cdot H$ values above 800 Hz·m in the case of models Fd and in the $f \cdot H$-range from about 750 to 1050 Hz·m in the case of models Fu. The amplitude of the transmitted wave (table) increases if the dip angle decreases. The differences between the transmissivity for the up-dipping and the down-dipping faults become evident when inspecting the curves calculated for dip angle 27°. In the case of the models Fu, low-frequency seam wave portions and high-frequency portions are transmitted with amplitudes which are higher the flatter the dipis. In contrast to this, in the case of the models Fd, low-frequency seam wave portions are transmitted with amplitudes which are lower the flatter the dipis. The opposite is valid for high-frequency seam wave portions: the flatter the dipis, the higher are the amplitudes. From averaging transmissivity values in the $f \cdot H$-range around 1100 Hz·m, we obtained values of 0.2 for a 27°-up-dipping fault plane and 0.4 for a 27°-down-dipping fault plane. These values indicate that for a high-frequency seam wave signal the difference between the maximum amplitudes of the transmitted waves might be distinct enough to allow for an identification of the dip type at least for flat dip angles.

Some of our fault models are similar to those investigated by Asten et al. (1984). These authors compared finite-element calculations with finite-difference simulations. For models containing vertical faults with differing throws, they proved agreement between the amplitudes in the reflection and transmission spectra and the normalized amplitudes evaluated by Korn and Stöckl (1982).

We also confirm the results obtained by Asten et al. (1984) (for comments on the conversion of the data, refer to Asten et al., 1984, Section 5). We obtained a value of 0.38 for the normalized amplitude of the seam wave reflected at the 63°-down-dipping fault plane [model Fd(3)], corresponding to an energy value of 14%. For the same fault type, Asten et al. (1984) gave values of about 13% for the reflected energy of the fundamental mode at the period (3.5 ms) where its Airy phase occurs.

Considering the effects of a fault zone with fractured rock, due to differences between our model Ez(2) and the model of Asten et al. (1984), only a rough comparison is possible. Both results indicate that the energy of the reflected seam wave is significantly higher than in the case of a simple fault and that the contribution of low-frequency seam wave phases to the reflection signal is increased.

From their investigations, Asten et al. (1984) deduced that the partition of energy between reflected and transmitted waves and between fundamental and higher modes characterizes the fault. This conclusion is based on a rather complete data set: Asten et al. (1984) calculated total energies of the reflected and transmitted seam waves scattered by the discontinuity in all directions. Furthermore, they considered energy values for the fundamental and higher modes in the $f \cdot H$-range from 200 to 3,000 Hz·m. Thus, these energy curves enable the discrimination of fault parameters, but they demand that data acquisition is not restricted to profile points in the coal and that broad-band field data are available.

In contrast, we used model data similar to field data: reflectivity and transmissivity curves are deduced from seismograms recorded in the centre of the model seam. Effects from mode conversions are negligible, because the Airy phases of the second and higher modes lie outside the $f \cdot H$-range in which seam waves are generated. In the field survey there exists a similar limit due to the frequency-band limitation of the equipment.

Although the reflectivity and transmissivity curves differ

significantly they are not particularly appropriate to make a clear-cut conclusion on the fault parameters. For example, no significant differences can be determined between the reflectivity and transmissivity curves for a fault with an offset of half a seam thickness and a fault with the same offset having a fault zone with an impedance of 3.5×10^5 g/(cm^{2}s). Or: the reflectivity curve for a vertical fault with a throw $s/H = 0.33$ is similar to the reflectivity curve for a 27°-down-dipping fault. In this latter case, the different curves for the transmissivity would allow the discrimination between the two fault types, if these data are available. On the other hand, if we have information on some of the fault parameters, e.g. the dip and the existence of a fault zone, we can estimate the third parameter, e.g. the throw, from the amplitudes.

Summary 4

Only if the throw is less than one seam thickness does it have an effect on the amplitude of the reflected seam wave: the amplitude decreases with the offset at the fault. The effect is strongest for high-frequency phases. The low-frequency phases of the transmitted seam wave are influenced by the fault only for throws larger than one seam thickness. The high-frequency phases depend on the throw even for offsets less than seam thickness.

For throws less than seam thickness, a fault zone with disaggregated or consolidated rock material leads to an increase in the amplitude of the reflected seam wave due to reflections from the interfaces coal-fault zone-coal.

Transmission of high-frequency seam waves is favoured by a down-dipping fault: there is an increase in the amplitudes of the transmitted seam wave with decreasing dip angle.

Discrimination of fault parameters on the basis of reflectivity and transmissivity curves is not reliable.

Conclusions

It was found that in seams with a dirt band, the Airy phase of the second mode, as well as Love seam wave phases which are part of the first mode, are excited. Interference of the two modes causes irregularities in the shapes and the amplitudes of the seam wave signals. This can lead to a deterioration of the results of data processing, especially for envelope-stacking and recompression. In extreme cases, two separate wave groups occurring in the reflection seismograms may lead to the false conclusion that two reflectors exist. With knowledge of the geological structure, one is able to calculate dispersion curves and curves of relative energy in order to decide whether higher modes are excited.

Our numerical results correspond to model data sets similar to those obtained from the currently employed field techniques. If the fault parameters can be estimated (e.g. from an opening in the roadway), the reflectivity and transmissivity curves presented and the normalized amplitudes can be exploited for a prognosis on the detectability of the fault.

However, a discrimination of fault parameters on the basis of reflectivity and transmissivity curves alone is not reliable, due to the ambiguity of the curves. Therefore, knowledge of some of the fault characteristics is also necessary in order to extract fault parameters from the field data. If such information is not available, the field data set must be supplemented, e.g. by measurements along vertical seismic profiles through the sequence rock-coal-rock.

Acknowledgements. This investigation has been carried out in cooperation with Bergbauforschung GmbH Essen, Prakla and Seismos GmbH Hannover, Ruhr-Kohle AG – BAG-Lippe Herne and Westfälische Berggewerkschaftskasse Bochum. Financial support was given by the BMFT and BMWi of the Federal Republic of Germany under the contract 'Flözwellenseismische Vorfelderkundung mit Hilfe digitaler Meßwerterfassung' and 'Einführung der Flözwellenseismik als Hilfsmittel zur Produktivitätssteigerung in den Betrieben des Steinkohlenbergbaus – Innovation III'. Dr. F.K. Brentrup, Dr. U. Klinge and Dr. H. Rüter gave valuable suggestions.

References

Alford, R.M., Kelly, K.R., Boore, D.M.: Accuracy of finite difference modelling of the acoustic wave equation. Geophysics **39**:834–842, 1974

Arnetzl, H.H.: Seismische Messungen untertage. Tagungsberichte 'Mensch und Maschine im Bergbau' der Gesellschaft Deutscher Metallhütten- und Bergleute, 133–141, 1971

Arnetzl, H.H., Klinge, U.: Erfahrungen mit der Flözwellenseismik bei der Vorfelderkundung. Glückauf **118**, 658–664, 1982

Asten, M.W., Drake, L.A., Edwards, S.: In-seam seimic Love wave scattering modeled by the finite element method. Geophys. Prosp. **32**, 649–661, 1984

Boore, D.M.: Love waves in nonuniform waveguides: finite difference calculations. J. Geophys. Res. **75**, 1512–1527, 1970

Boore, D.M.: Finite difference methods for seismic wave propagation in heterogeneous materials. In: Methods in computational physics, Vol. 11, B. Alder, S. Fernbach, M. Rotenberg, eds. New York: Academic Press 1972

Brentrup, F.K.: Flözwellenseismische Vorfelderkundung. Glückauf **115**, 820–823, 1979

Buchanan, D.J.: In-seam seismology: A method for detecting faults in coal seams. In: Developments in geophysical exploration methods, Vol. 5, A.A. Fitch, ed. London and New York: Applied Science Publishers Ltd., 1983

Dresen, L., Freystätter, S.: Rayleigh channel waves for the in-seam seismic detection of discontinuities. J. Geophys. **42**, 111–129, 1976

Dresen, L., Kerner, C., Kühbach, B.: The influence of an asymmetry in the sequence 'rock-coal-rock' on the propagation of Rayleigh seam-waves. Geophys. Prosp. **33**, 519–539, 1985

Dziewonski, A.M., Hales A.L.: Numerical analysis of dispersed seismic waves. In: Methods in computational physics, Vol. 11, B. Alder, S. Fernbach, M. Rotenberg, eds. New York: Academic Press, 1972

Edwards, S., Asten, M.W., Drake, L.A.: P-SV wave scattering by coal seam inhomogeneities. Geophysics **50**, 214–223, 1985

Fertig, J.: Ebene Wellen in geschichteten Medien. Beitrag zum Seminar: "Numerische Methoden für seismische Wellenausbreitung und elektromagnetische Induktion", Neustadt, 1982

Kerner, C.: Untersuchungen an zweidimensionalen analogen und numerischen Modellen zur Transmission und Reflexion von Love- und Rayleigh-Flözwellen. Ph.D. thesis, Berichte des Institutes für Geophysik der Ruhruniversität Bochum, Series A, No. 14, Bochum, 1984

Kerner, C.: Simulation der Ausbreitung von seismischen Wellen in Wellenkanälen mit Hilfe der Methode der finiten Differenzen. Conferences on Cyber 205, Proceedings, H. Ehlich, K. Schlosser, eds., Bochum, 1985

Korn, M., Stöckl, H.: Reflection and transmission of Love channel waves at coal seam discontinuities computed with a finite difference method. J. Geophys. **50**, 171–176, 1982

Krey, Th.: Channel waves as a tool of applied geophysics in coal mining. Geophysics **28**, 701–714, 1963

Küpper, F.J.: Theoretische Untersuchungen über die Mehrfachaufstellung von Geophonen. Geophys. Prosp. **6**, 194–256, 1958
Millahn, O.: Flözwellenseismik. Prakla-Seismos Report 2 + 3, Hannover, F.R. Germany, 19–30, 1980
Räder, D., Schott, W., Dresen, L., Rüter, H.: Calculation of dispersion curves and amplitude-depth distributions of Love channel waves in horizontally layered media. Geophys. Prosp., 1985 (in press)
Reynolds, A.C.: Boundary conditions for the numerical solution of wave propagation problems. Geophysics **43**, 1099–1110, 1978
Rüter, H., Schepers R.: In-seam seismic methods for the detection of discontinuities applied to West Germany coal deposits. In: Coal Exploration 2, Argall, G.O., ed.: pp 267–293, Proc. of 2nd Int. Cool Exploration Symposium; San Francisco: Miller-Freeman, 1979

Received November 6, 1984; revised version April 12, 1985
Accepted April 25, 1985